Improved value for the silicon intrinsic carrier concentration from 275 to 375 K

A. B. Sproul and M. A. Green
Centre for Photovoltaic Devices and Systems, University of New South Wales, Kensington, Australia 2033

(Received 4 September 1990; accepted for publication 4 April 1991)

A recent review has suggested that the commonly cited value of 1.45×10^{10} cm^{-3} for the silicon intrinsic carrier concentration at 300 K is inconsistent with the best experimental data. An alternate value of 1.08×10^{10} cm^{-3} was proposed. From measurements of the current-voltage characteristics of *p-n* junction diodes, this paper reports a new and more accurate determination of this parameter over the 275–375 K temperature range which supports such lower values. The one-standard-deviation uncertainty in the measurement of the intrinsic carrier concentration is estimated to lie in the 3%–4% range, about three times smaller than previous measurements at these temperatures. Additionally, this technique provides information on the minority carrier electron diffusivity in silicon.

I. INTRODUCTION

The intrinsic carrier concentration n_i is an important parameter in semiconductor device physics.[1] Minority carrier densities and recombination properties, which are of prime importance for the modeling of many semiconductor devices, both depend on n_i. In a recent review,[2] the commonly cited value of 1.45×10^{10} cm^{-3} (Refs. 1, 3, and 4) for the intrinsic carrier concentration of silicon at 300 K was shown to be inconsistent with the best experimental data. An alternate value of $1.08(8)\times10^{10}$ cm^{-3} was deduced. The digit in parentheses represents the estimated one-standard-deviation (1σ) uncertainty in the last digit of the previous value, a convention adopted throughout this paper. An inconsistency of this magnitude is significant in silicon device analysis. Use of the larger value would lead to an overestimation of the minority carrier current flows in a device for a given voltage by a factor of approximately 2.

There have been a number of measurement techniques previously employed for determining the intrinsic carrier concentration of silicon.[2] The most direct method used has been the measurement of the conductivity of silicon at relatively high temperatures where it has intrinsic properties. If the electron and hole mobilities are known, the intrinsic concentration can then be determined. However, measurement of mobilities is most readily made at lower temperatures where the material has extrinsic properties. Hence the conductivity and mobility measurements are usually made at different temperatures. This introduces some degree of uncertainty in the determination of n_i due to the extrapolations involved (estimated uncertainty of 8% near room temperature using the best available data[2]). A second method is based on the measurement of the conduction and valence-band density-of-states effective masses and the band gap of silicon. This method has an estimated uncertainty near room temperature of 11%,[2] primarily due to the uncertainties associated with the interpretation of hole effective mass measurements made at low temperatures. A third method involves the measurement of the characteristics of semiconductor devices. However, in a past study[5] the devices used were *p-i-n* junction diodes designed to operate in high injection which limits the accuracy of the determination of n_i.[2]

The method described in this work involves the measurement of injected minority carrier current flows in narrow base *p-n* junction diodes. The devices studied were constrained to operate in low injection. Only a small number of parameters is needed to describe the data, allowing n_i to be determined with an estimated uncertainty of only 3% near room temperature. Preliminary results at 300 K have recently been reported.[6] In this paper a more complete description of the measurements, analysis, and error estimates are reported, together with results over the 275–375 K temperature range. The value at 300 K determined in this work is $1.00(3)\times10^{10}$ cm^{-3} which is consistent with the value of $1.08(8)\times10^{10}$ cm^{-3} mentioned above[2] and with the value of 1.02×10^{10} cm^{-3} reported by Wasserab.[7] However, it does not support the commonly cited value of 1.45×10^{10} cm^{-3} (Refs. 1, 3, and 4) of uncertain origin.[2]

II. EXPERIMENT

The improvement in accuracy reported in this paper was made possible by recent progress in high efficiency silicon photovoltaics. The devices used in this study were based on the passivated emitter and rear cell (PERC), the first silicon solar cells to surpass 23% energy conversion efficiency.[8] These devices are well suited to measurements of this type as they are large area devices (4 cm^2) with low junction leakage, near-ideal junction characteristics, high postprocessing carrier lifetimes, and low recombination rates at surfaces and in diffused regions. Additionally, they have an unusual rear contacting scheme involving small contact areas with high recombination velocity interposed within areas with low recombination velocity.[8]

In order to simplify the analysis, device design was streamlined by using a planar, rather than the normally textured,[8] top surface (Fig. 1). The optional second heavy phosphorus diffusion under the top surface metalization[8] was also not incorporated. The oxide passivated rear sur-

 0021-8979/91/020846-09$03.00

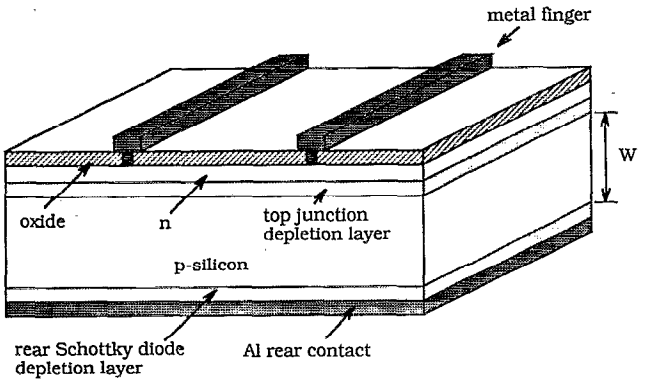

FIG. 1. Modified PERC silicon solar cell structure. W is the width of the quasineutral p region.

face with small area Al contacts was replaced by an evaporated Al layer completely covering the wafer rear. The rear metalization was not subjected to any high-temperature steps other than the standard subeutectic treatment at 400 °C for 5 min in a 5% H_2/N_2 atmosphere.[8] All other aspects of the high efficiency PERC structure were retained. The device substrates were high lifetime, float zone, (100) p-type, boron-doped, silicon wafers with nominal resistivities of 100, 10, 2, and 0.5 Ω cm, polished on both surfaces.

The short-circuit current (I_{SC}) vs open-circuit voltage (V_{OC}) of the devices was measured at varying light intensities. By investigating the I_{SC} vs V_{OC} rather than dark current-voltage behavior, the cell series resistance need not be determined. The meters used for the measurement of I_{SC} and V_{OC} were found to have an accuracy of 0.2% and 0.02% for the current and voltage measurements, respectively, when calibrated against standards. The temperature of the device was maintained constant using a temperature controlled copper block. A Peltier device was used to heat or cool the block as required and a thermistor embedded in the block was used to monitor and control the temperature.

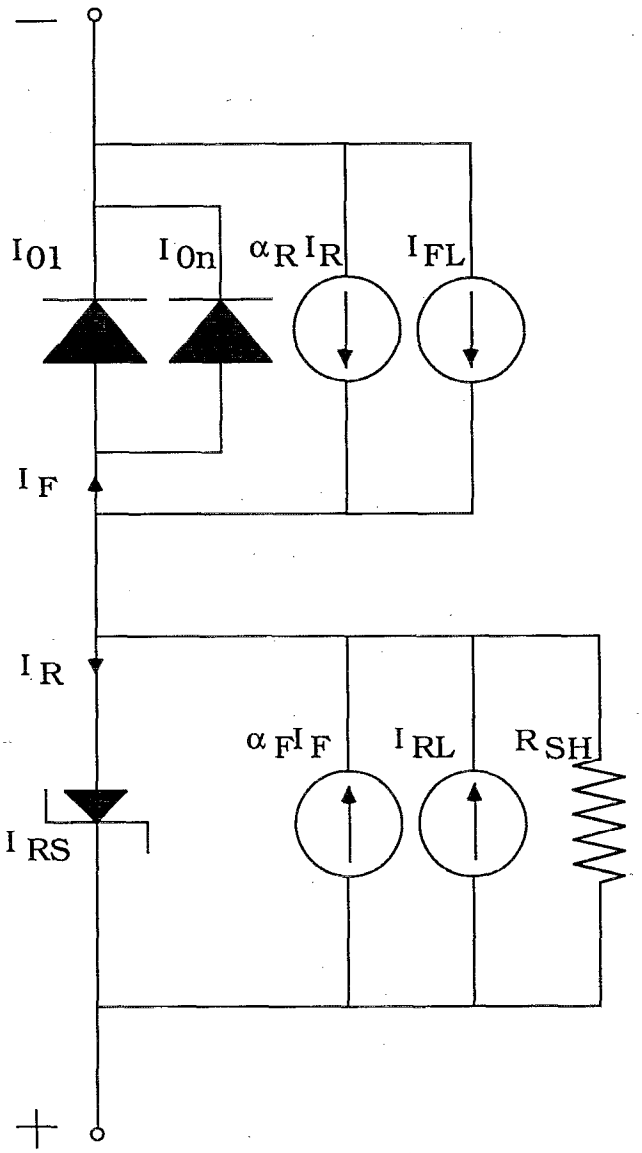

FIG. 2. Modified Ebers-Moll circuit describing the PERC cell.

III. THEORY

In order to determine the intrinsic carrier concentration from the measured $I_{SC} - V_{OC}$ values, the devices were modeled using standard semiconductor device theory. From Fig. 1, it can be seen that the device structure is essentially a p-n junction diode. As indicated in Fig. 1, Al evaporation on the polished rear of the wafer gives a rectifying Schottky diode along this surface with a relatively low barrier height of 0.4–0.6 eV.[1] The chosen sintering conditions produce partial shunting of this diode. The device structure can be modeled as a bipolar transistor with the diffused top junction forming the emitter and the rear Schottky junction forming the collector. The collector is connected to the base (the p-type substrate) by the relatively low shunting resistance produced by sintering.[8]

These devices were modeled using a modified Ebers-Moll equivalent circuit[1,8] shown in Fig. 2. The diode symbols represent diodes associated with the top and rear junctions.[1] The top junction is modeled by two diodes having ideality factors of unity and n, where n is greater than unity.[9] I_{01} and I_{0n} are the saturation currents associated with each of these two diodes. I_{RS} is the saturation current associated with the rear junction. All three saturation currents have to be calculated with the other junction shorted, i.e., the junction area replaced by an infinite recombination velocity surface.[1] Also shown are the normal current-controlled current sources of the Ebers-Moll equivalent circuit.[1] These current sources have values of $\alpha_F I_F$ and $\alpha_R I_R$, determined by the current flowing in the opposite junction multiplied by the injection efficiency α of the opposite junction.[1]

To the normal Ebers-Moll circuit has to be added an additional current source across each junction to model photogenerated current. The values assigned to these sources, I_{FL} and I_{RL}, correspond to the current flowing to

the respective junction at short circuit with the opposite junction also short circuited. Also added to the equivalent circuit is a shunt resistance (R_{SH}) across the rear junction to model the shunting resistance discussed previously.

When this shunting resistance is small, the voltage across the rear junction is held low as is the current I_R through the rear junction. In this case the Ebers-Moll model gives

$$I_{SC}=I_{01}\left\{\exp\left[\frac{q}{kT}(V_{OC}+I_{SC}R'_{SH})\right]-1\right\}+I_{0n}\left\{\exp\left[\frac{q}{nkT}(V_{OC}+I_{SC}R'_{SH})\right]-1\right\}. \tag{1}$$

The ideality factor n describes recombination within the space-charge region at the top junction and depleted (or inverted) surface regions. This description is valid for devices operating in low injection only. The thermal voltage kT/q equals 25.852 16(22) meV at 300 K using recommended values of the physical constants.[10] R'_{SH} is an effective resistance describing the effect of the actual shunt resistance, R_{SH}, of the rear Schottky diode and also that of current collected by this diode at short circuit as given by

$$I_{SC}R'_{SH}=(\alpha_F I_{FL}+I_{RL})R_{SH}. \tag{2}$$

I_{01} is strongly dependent upon n_i.[1] For a one-dimensional model of the cell the relationship is given by

$$I_{01}=I_{0b}+I_{0e}, \tag{3}$$

where

$$I_{0b}=\frac{AqD_n n_i^2}{WN_A^-}\left[\frac{W}{L_n}\coth\left(\frac{W}{L_n}\right)\right]. \tag{4}$$

I_{0b} is the saturation current associated with the p region and rear contact while I_{0e} is the saturation current associated with the front n-type surface diffusion and metalization. A is the area of the cell; q is the electronic charge; D_n, L_n, and N_A^- are the minority carrier electron diffusivity, diffusion length, and ionized dopant concentration in the p-type substrate, respectively, and W is the width of the quasineutral p region (Fig. 1).

The previous analysis describes the one-dimensional current flow of a p-n junction. In the actual device the value of I_{01} determined experimentally will be slightly greater than that described by Eqs. (3) and (4). This is due to the minority carrier electron current spreading from the periphery of the p-n junction as it is injected into the base region. This occurs because the top junction is smaller in area than the rear contact for the planar top junction structure used. This results in the actual value of I_{0b} being greater than that described by Eq. (4), as shown below. For I_{0e} this "fringing effect" is negligible as the width of the emitter is very much less than the lateral dimensions of the cell.

An analytical solution for the minority current flows in the base region, in terms of Bessel functions, has been found by Chen *et al.*[11] The geometry considered is circular with the oxide-substrate interface at the boundary of the cell having a surface recombination velocity of zero. For the present devices, since the diffusion length $L_n \gg W$, the equation to be solved to calculate bulk minority carrier distributions and hence peripheral current effects, approaches Laplace's equation, simplifying the analysis. Moreover, since the lateral dimensions of the cell has a length $a=2$ cm and $a \gg W$ this fringing effect is small. The solution of Laplace's equation for the square geometry considered here, gives a correction to I_{0b} to first order in W/a, of[12]

$$I_{0bf}=I_{0b}\left(1+\frac{W}{a}\frac{8\ln 2}{\pi}+\text{higher order terms in }\frac{W}{a}\right). \tag{5}$$

I_{0bf} is the saturation current density associated with the base region which includes the fringing effect. Evaluating this expression for $W=280$ μm and $a=2$ cm, the bracketed term has a value of 1.025. This is in good agreement with the value given in Ref. 11 for a circular geometry of the same periphery to area ratio. The accuracy of the above expression can be estimated from the magnitude of the higher order terms which are well known for the circular geometry.[13] Evaluating these terms implies that this correction is accurate to within 0.5%.

Another aspect that needs to be considered is the possibility of peripheral effects at the surface. The top surface of the device has a planar structure with the 4-cm^2 diffused area surrounded by the oxidized surface of the p-type substrate. This p-type surface could be inverted or depleted resulting in additional peripheral effects.[14] If depleted, enhanced recombination in these peripheral regions could decrease V_{OC}. However, the relative effectiveness of recombination in such depleted regions decreases with increased illumination level.[15] Hence, if the surface is depleted, peripheral effects would be apparent as an $n>1$ term in the $I_{SC}-V_{OC}$ characteristics. As only the $n=1$ component is extracted and used in the subsequent analysis, depleted peripheral regions will have no influence on the results.

If the surface is inverted, the effective area of the diode is enhanced since electron current can flow laterally along the inversion layer as along the top diffused layer.[14] As the illumination level increases, this lateral communication becomes increasingly less effective due to the increased ohmic drops along the relatively high sheet resistivity inversion layer. Again this effect would be apparent as an $n>1$ term in the $I_{SC}-V_{OC}$ characteristics which would have no influence on the extracted results. Additionally, it is unlikely that the surface is accumulated as the substrates used are p-type and oxides are, in general, positively charged.[1]

It is concluded that, regardless of peripheral surface conditions, only the "fringing field" effect will influence the $n=1$ current component I_{01}. The initially deduced values of I_{0b} were reduced by a factor of 1.025(5) to extract the "one-dimensional" value modeled by Eq. (4).

Rearranging Eqs. (3) and (4) and including the fringing field effect as discussed above, the intrinsic carrier concentration is then given by

TABLE I. Saturation current I_{01}, ionized dopant density N_A^-, diffusivity D_n, diffusion length correction factor $\omega \coth \omega$, and experimental value of the intrinsic carrier concentration n_i at temperatures of 275, 300, 325, 350, and 375 K derived from cell measurements upon wafers of the nominal resistivity ρ indicated. Emitter saturation current I_{0e} at 275–375 K is 3.4(15) fA, 0.28(12) pA, 12(5) pA, 0.30(13) nA, and 4.8(20) nA, respectively. Width of the quasineutral p region W for wafers of resistivity of 100, 10, 2, and 0.5 Ω cm is 278(3), 284(3), 284(3), and 280(3) μm, respectively, and 281(3) for the additional 2-Ω cm wafer investigated at 300 K which is marked with an asterisk.

T (K)	ρ (Ω cm)	I_{01} (A)	N_A^- (10^{14} cm^{-3})	D_n (cm^2/s)	$\omega \coth \omega$	n_i (cm^{-3})
275	100	$7.24(43)\times10^{-12}$	1.42(8)	41.5(21)	1.003(4)	$1.02(5)\times10^{9}$
	10	$7.52(45)\times10^{-13}$	13.5(7)	38.8(22)	1.003(4)	$1.06(5)\times10^{9}$
	2	$1.34(8)\times10^{-13}$	68.8(36)	34.3(33)	1.007(6)	$1.06(7)\times10^{9}$
	0.5	$2.37(14)\times10^{-14}$	360(20)	26.3(59)	1.040(40)	$1.07(13)\times10^{9}$
300	100	$5.76(20)\times10^{-10}$	1.42(8)	36.6(18)	1.003(3)	$9.72(40)\times10^{9}$
	10	$5.90(21)\times10^{-11}$	13.5(7)	34.6(20)	1.003(3)	$9.94(40)\times10^{9}$
	2	$1.16(4)\times10^{-11}$	68.8(36)	31.1(30)	1.007(4)	$1.04(6)\times10^{10}$
	2*	$1.14(4)\times10^{-11}$	69.7(36)	31.0(30)	1.007(4)	$1.03(6)\times10^{10}$
	0.5	$2.05(7)\times10^{-12}$	362(20)	24.5(55)	1.040(30)	$1.03(12)\times10^{10}$
325	100	$2.48(11)\times10^{-8}$	1.42(8)	32.5(16)	1.003(4)	$6.76(30)\times10^{10}$
	10	$2.56(11)\times10^{-9}$	13.5(7)	31.1(18)	1.003(4)	$6.90(32)\times10^{10}$
	2	$5.01(22)\times10^{-10}$	68.9(36)	28.5(28)	1.007(6)	$7.13(43)\times10^{10}$
	0.5	$9.01(39)\times10^{-11}$	363(20)	23.4(52)	1.040(40)	$7.05(84)\times10^{10}$
350	100	$6.07(30)\times10^{-7}$	1.42(8)	29.2(15)	1.003(4)	$3.53(16)\times10^{11}$
	10	$6.40(32)\times10^{-8}$	13.5(7)	28.2(16)	1.003(4)	$3.62(17)\times10^{11}$
	2	$1.27(6)\times10^{-8}$	68.9(36)	26.2(25)	1.007(7)	$3.74(23)\times10^{11}$
	0.5	$2.24(11)\times10^{-9}$	364(20)	22.2(50)	1.040(50)	$3.62(44)\times10^{11}$
375	100	$9.76(52)\times10^{-6}$	1.42(8)	26.4(13)	1.003(4)	$1.49(7)\times10^{12}$
	10	$1.08(6)\times10^{-6}$	13.5(7)	25.8(15)	1.003(4)	$1.56(8)\times10^{12}$
	2	$2.13(11)\times10^{-7}$	69.0(36)	24.3(24)	1.007(8)	$1.59(10)\times10^{12}$
	0.5	$3.81(20)\times10^{-8}$	365(21)	21.1(48)	1.040(60)	$1.54(19)\times10^{12}$

$$n_i = \sqrt{\frac{WN_A^-}{AqD_n}\,\frac{(I_{01}-I_{0e})}{1.025}\,\frac{1}{[(W/L_n)\coth(W/L_n)]}}. \tag{6}$$

Hence, by measuring the saturation current I_{01} and the other parameters in Eq. (6), a value for n_i can be determined. To obtain I_{01} from the experimental $I_{SC} - V_{OC}$ data, Eq. (1) was fitted to the data with I_{01}, I_{0n}, n, and R'_{SH} being the variable parameters. The methods used to measure the other parameters and the associated uncertainties for all parameters are discussed in the following section.

IV. RESULTS AND ERROR ESTIMATES

A. Output characteristics

Devices were fabricated on 100-, 10-, 2-, and 0.5-Ω cm substrates. The $I_{SC} - V_{OC}$ characteristics of all devices were measured at temperatures of 275.0(3), 300.0(2), 325.0(3), 350.0(4), and 375.0(5) K. At 300.0(2) K, ten cells fabricated on five different wafers were investigated while at all other temperatures eight cells on four wafers were studied. An additional 2-Ω cm device was investigated at 300.0(2) K. The results for this device is marked with an asterisk in Table I.

The characteristics of the 100-, 10-, 2-, and 0.5-Ω cm cells at 300.0(2) K are shown in Fig. 3. (Data for only one of the 2-Ω cm samples are plotted as the other sample has virtually identical characteristics, differing by $<0.5\%$.) The results for the 10-Ω cm device are shown in Fig. 4 for the range of temperatures investigated and are typical for all the devices. The data are well described by Eq. (1) with an accuracy of $\sim 1\%$ for all devices at all temperatures. For the 100-Ω cm cell at 300.0(2) K, data above 450 mV were excluded as high injection is approached and the previous analysis becomes invalid. At all temperatures device characteristics that approached the calculated high injection level were excluded from the analysis.

The deviation of the measured characteristics in Figs. 3 and 4 from a slope corresponding to an ideality factor of unity occurs most markedly at high values of I_{SC}. This deviation is due to the increasing voltage across the rear Schottky diode as incorporated into Eq. (1). In Fig. 3, this

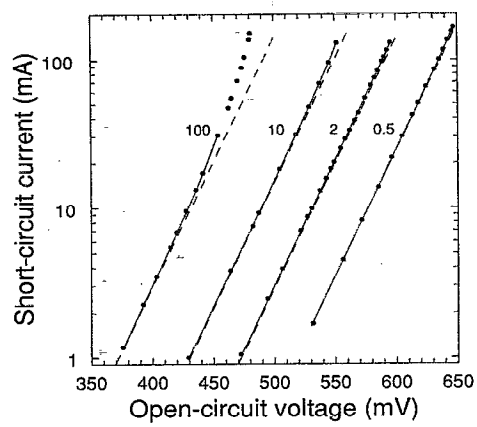

FIG. 3. The measured I_{SC}-V_{OC} characteristics (closed circles) of the cells for different resistivities (100, 10, 2, and 0.5 Ω cm) at 300.0(2) K. The solid line is a fitted curve while the dashed line is the ideal component of this fitted curve (ideality factor $n=1$).

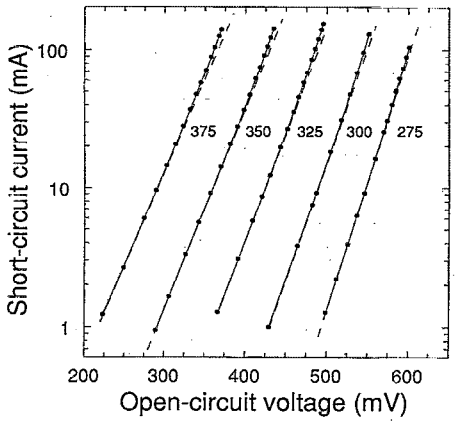

FIG. 4. The measured I_{SC} — V_{OC} characteristics (closed circles) of the 10-Ω cm device at 275.0(3), 300.0(2), 325.0(3), 350.0(4), and 375.0(5) K. The solid line is a fitted curve while the dashed line is the ideal component of this fitted curve (ideality factor $n=1$).

deviation is least for the 0.5-Ω cm and greatest for the 100-Ω cm device since the rear junction in the latter is more difficult to shunt due to the increase in depletion layer width for lightly doped substrates. However, as seen from Figs. 3 and 4, the I_{01} component (dashed lines) dominates over the measured range reducing the uncertainty in its determination.

B. Saturation current I_{01} and temperature

The values of I_{01} for all devices and temperatures are given in Table I as well as the associated 1σ uncertainty. Uncertainty in I_{01} arising from its extraction from the measured I_{SC} — V_{OC} data is estimated at $<2\%$ due to the dominance of the I_{01} component. An uncertainty of 0.5% in I_{01} was incorporated due to the fringing field corrections discussed in Sec. III.

Additional uncertainty arises from uncertainty in measurement of the device temperature. The thermistor used to control block temperature allowed the temperature to be set to within 0.1 °C precision and it maintained block temperature constant during the measurements to within 0.1 °C. The accuracy of the resulting set temperature was measured using a Type K thermocouple calibrated using ASTM recommended procedures.[16] The estimated accuracy of this calibration is 0.1 °C. Additional uncertainty in the temperature arises from temperature gradients across the surface of the wafer under test conditions. These gradients arise from the copper block which has temperature gradients towards its edge due to heat exchange with the ambient. These effects were minimal for measurements near room temperature. The total estimated uncertainty in temperature ranged from 0.2 °C for measurements near room temperature to 0.5 °C at 375 K. The uncertainty was incorporated into the analysis as an uncertainty in I_{01} at the nominal measurement temperature. The measured temperature dependence of I_{01} can be described quite accurately by an equation of the form $A\,e^{-B/T}$. dI_{01}/dT is then described by the expression $I_{01}(14670/T^2)$. This gives uncertainties in the range of 10.4 to 19.4%/K for 375 to 275 K, respectively, that are included in Table I.

An additional small uncertainty in I_{01} arises from the increase in cell temperature with increasing illumination level. This causes the V_{OC} to decrease and has greatest effect at the higher values of I_{SC}. The effect was investigated by monitoring the V_{OC} of a device over the period spanning the initial illumination of the cell and the eventual stabilization of V_{OC}. While monitoring V_{OC}, the block was maintained at a constant temperature. This change in V_{OC} is directly proportional to the temperature (about -2 mV/°C). The temperature rise was found to increase approximately linearly with I_{SC} reaching 0.8 °C at the maximum current investigated (200 mA) and being negligible below 25 mA. Correcting for this temperature effect, however, was found not to greatly influence the extracted value of I_{01}, with the corresponding additional uncertainty estimated as 0.5%.

C. Ionized substrate doping level N_A^-

In order to determine N_A^-, four-point-probe resistivity measurements upon substrates were made at 23 °C and converted to dopant concentrations, N_A, at 300 K using the results of Thurber *et al.*[17] Spreading resistance and capacitance-voltage techniques gave consistent results. Although only a small effect, the fraction of ionized dopants as a function of temperature was calculated by solving the charge balance equation for the Fermi energy (E_F) using an iterative procedure. For the range of temperatures and dopant concentrations considered the hole density in the p region is given by[1]

$$p \approx N_A^-, \tag{7}$$

where

$$N_A^- = \frac{N_A}{1 + g \exp[(E_A - E_F)/kT]} \tag{8}$$

and

$$p = N_V \exp\left[\frac{E_V - E_F}{kT}\right]. \tag{9}$$

g is the degeneracy factor for acceptor levels, commonly assigned a value of 4.[1] Differing values appear in the literature, notably that employed by Li,[18] whose ionization values are used by Thurber *et al.*[17] However, the results presented here are unaffected by values of g between 2 and 6. E_V is the energy at the top of the valence band, N_V is the density of states of the valence band, and E_A is the acceptor ionization energy which for boron-doped silicon can be expressed by[18]

$$E_A = E_V + 0.0438 - 3.037 \times 10^{-8} N_A^{1/3}. \tag{10}$$

The more recent values of the hole effective mass deduced by Green[2] were used in calculating N_V, giving similar values for N_A^- to those of Li.[18] The difference between these values was included as an uncertainty in N_A^- amounting to 2% for the worst case for the 0.5-Ω cm sample. Uncertainties between 1.5% to 2.5% were assigned to

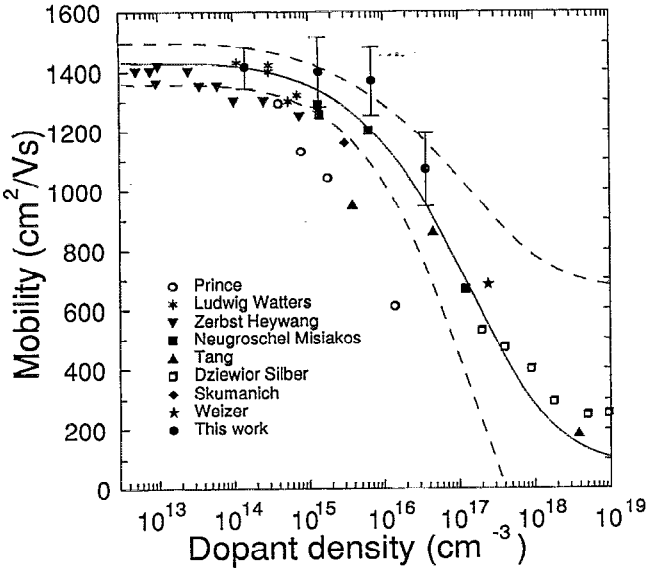

FIG. 5. Minority carrier electron mobility in silicon as a function of dopant density at 300 K as reported by a number of investigators. The solid line is the majority carrier values (Ref. 16) and the dashed lines are the one-standard-deviation uncertainty assigned to the minority carrier values (assuming the minority carrier mobility is equal to the majority carrier mobility).

the four-point-probe resistivity measurements and 5% assigned to the conversion from resistivity to dopant density based on estimated total error by Thurber *et al.*[17] The total uncertainty is given in Table I.

D. Minority carrier diffusivity D_n

There are relatively few reports of experimental values of the minority carrier diffusivity D_n, or equivalently, the minority carrier mobility μ_n (since $D_n = \mu_n kT/q$).[19,20] A plot of μ_n vs dopant density at 300 K is shown in Fig. 5 with data from a number of investigators.[21–29] Some of the doping density values have been reevaluated using a more accurate conductivity-doping density conversion than was initially employed. Most of the data lie close to the majority carrier values (solid line) as reported by Thurber *et al.*[17] except for the early data of Prince[21] and, more recently, a single point reported by Tang *et al.*[26] Early values of μ_n were also reported by Cronemeyer,[30] Ludwig and Watters,[22] and Zerbst and Heywang[23] which used the same method as, and were in fair agreement with, Prince. Some possible reasons for this discrepancy is the technique initially employed[27] or that the material available may have been of low purity.[24] The material may have contained a high degree of defects or have had a high level of compensation resulting in a decrease in the measured mobility. A further possibility is that the mobility was reduced due to the electric fields used in the early drift mobility experiments.[21–23,30] Recently, it has been observed that in the presence of moderate electric fields (<200 V/cm), the minority carrier mobility is less than the zero-field measurements.[26] This effect has been attributed to electron-hole (*e-h*) scattering.[26] In the presence of an electric field, the electrons and holes have opposite average drift velocities. The transfer of momentum during *e-h* collisions, from the majority to the minority carriers, leads to a reduction in the minority carrier mobility.[31]

The value reported by Tang *et al.*,[26] at a doping density of 3.8×10^{15} cm^{-3}, is also lower than the majority values. This data point, however, is in the region of lowest accuracy of the method employed and all other values reported are close to the majority values. He concludes the point is in reasonable agreement with the majority value despite the fact that his value is only 75% of the latter. Values reported for a large number of samples[30,32] showed considerable scatter. However, the average values in the latter study[32] are again close to the majority values.

The approach taken in this work was to assume that, within experimental error, the minority carrier D_n has the same value as for majority carriers.[17] This would seem, on theoretical grounds, to be a good assumption for the lightly doped specimens (e.g., the 100-Ω cm device) as lattice scattering then determines transport properties. As doping increases, scattering by the ionized impurities overrides lattice scattering. As reported by Dziewior and Silber,[27] at high doping levels, μ_n for minority carrier electrons can then deviate quite substantially from the majority carrier values.

A conservative estimate of the maximum likely error in D_n was made based on 75% of the difference between D_n in intrinsic silicon and the value of D_n at a particular value of the dopant density. An additional 5% measurement error was attributed to the determination of the majority carrier values. This maximum likely error was converted to a 1σ uncertainty using a technique employed in estimating uncertainties in the recommended values of the physical constants.[10] A quantity denoted as the semirange a is assigned to the maximum likely error for a parameter. The equivalent variance is then taken to be $a^2/3$ and from this the standard deviation can be calculated. This uncertainty is plotted in Fig. 5 (dashed lines) and included in Table I. Note, all experimental data lie within or close to the 1σ uncertainty bound with the exception of that of Prince and Tang, as previously discussed.

The temperature variation of D_n was calculated by considering the variation of resistivity of n-type silicon with temperature.[33] For the temperature range and doping densities considered the resistivity is given by[33]

$$\rho_n=\rho_{n0}\left(\frac{T}{T_0}\right)^{\alpha}=\frac{1}{q\mu_n N_D^+}, \tag{11}$$

where

$$\alpha=296.15C_T. \tag{12}$$

ρ_n and ρ_{n0} are the resistivity at temperatures T and T_0 where T_0 is equal to 296.15 K (23 °C). α is a function of resistivity and is related to the coefficient of resistivity C_T by Eq. (12). Values of C_T were taken from Table V of Ref. 34. The mobility, and hence the diffusivity, was then calculated from Eq. (11) using the appropriate values of N_D^+. These were calculated for the donors in a similar way as outlined previously for N_A^-, after Li *et al.*[35] Again the

TABLE II. The intrinsic carrier concentration of silicon as a function of temperature for three different experimental methods. Saturation current: this work; intrinsic conductivity (Ref. 2); and band parameters (Ref. 2). The three sets of results calculated from band parameters are based on hole effective mass parameters from different investigators. The error estimates in these cases are based on a 15% uncertainty in the value of these effective masses (Ref. 2).

T (K)	Units	Saturation current	Intrinsic conductivity	Band parameters		
				Madarasz	Hensel	Humphreys
275	10^9 cm^{-3}	1.05(4)	1.14(14)	1.12(13)	1.04(12)	1.21(14)
300	10^{10} cm^{-3}	1.00(3)	1.09(9)	1.07(13)	0.99(12)	1.16(14)
325	10^{10} cm^{-3}	6.90(24)	7.22(43)	7.42(87)	6.87(81)	8.04(94)
350	10^{11} cm^{-3}	3.61(13)	3.70(23)	3.93(47)	3.63(43)	4.25(51)
375	10^{12} cm^{-3}	1.54(6)	1.57(10)	1.67(20)	1.55(19)	1.81(22)

effective mass values deduced by Green[2] were used. Uncertainties in D_n, at all temperatures, were assigned using the same method as outlined above for the 300-K data. The uncertainties associated with the calculation of donor ionization were negligible in comparison to those in D_n.

E. Minority carrier diffusion length L_n

The value of L_n does not have to be determined accurately since the term in square brackets in Eq. (6) (the diffusion length correction factor) will be close to unity provided L_n is greater than W. By comparing the saturation currents I_{01} of present devices with the I_{01} of normal cells with the rear partially contacted, a lower bound can be placed on L_n.[8] This lower bound is smallest for the 0.5-Ω cm device, although even then nearly twice the wafer thickness. An upper bound on L_n can be determined in a similar way by attributing 10% of I_{01} of the normal cell to recombination associated with L_n. This allows the uncertainty in the correction term to be estimated. In the worst case for the 0.5-Ω cm cell this uncertainty is only 6% and for all other devices it is negligible.

F. Quasineutral width W and cell area A

W and A were measured with $<1\%$ uncertainty using a micrometer and a calibrated optical microscope. In order to determine the width of the quasineutral p region, W, the depth of the junction (based on spreading resistance measurements for similarly processed devices) and the calculated depletion widths associated with the front and rear junction were subtracted from the measured substrate thickness. The values of W are 278(3), 284(3), 284(3), and 280(3) μm for the 100-, 10-, 2-, and 0.5-Ω cm samples, respectively, and 281(3) μm for the additional 2-Ω cm device investigated at 300 K.

G. Emitter saturation current I_{0e}

I_{0e} is the smallest term in Eq. (6) and was estimated from the high V_{OC} of normal PERC cells as a function of temperature.[36] The values assigned to I_{0e} were 3.4(15) fA, 0.28(12) pA, 12(5) pA, 0.30(13) nA, and 4.8(20) nA at 275, 300, 325, 350, and 375 K, respectively. The uncertainty assigned to I_{0e} was conservatively estimated at $\sim 40\%$. This large uncertainty has only a small effect on the value of n_i extracted, as I_{0e} is small in comparison to I_{01}.

H. Other uncertainties

Additional uncertainty arises from differences between the experimental structure and that modeled by Eq. (1). The largest source of such uncertainty may arise from lateral and vertical variations in N_A^- and D_n. There is some evidence for enhanced diffusivity near the junction due to local stress.[37] The present devices have lightly diffused emitters which would minimize this effect.[37] An additional 1σ uncertainty of 3% is included into error estimates to accommodate such spatial variations.

V. DISCUSSION

The present results for n_i are shown in Table I together with 1σ uncertainty estimates in this value and other parameters of Eq. (6). The values from all the wafers are in good agreement with one another for all temperatures. A weighted average of the results at each temperature, accounting for correlated and uncorrelated uncertainties, is shown in Table II with 1σ uncertainties. The results can be described to within 3% by the expression deduced by Wasserab:[7]

$$n_i = 5.71\times 10^{19}\left(\frac{T}{300}\right)^{2.365}\exp\left(\frac{-6733}{T}\right)\ \text{cm}^{-3}. \quad (13)$$

The agreement here may be fortuitous as this expression is based on conductivity measurements made at 500 to 1000 K and around 300 K has an estimated uncertainty of 20%.[2] An expression of the same form describes the data of the present paper to within 0.5% and is given by

$$n_i = 9.15\times 10^{19}\left(\frac{T}{300}\right)^{2}\exp\left(\frac{-6880}{T}\right)\ \text{cm}^{-3}. \quad (14)$$

The results described here are also in good agreement with the values deduced from measurements of band parameters and intrinsic conductivity measurements[2] as shown in Table II. The uncertainty estimates of $<4\%$ are, however, considerably smaller in the present case. The agreement improves at the upper region of the temperature range considered where the intrinsic conductivity method becomes more accurate.

TABLE III. Ratio of diffusivity of the 10-, 2-, and 0.5-Ω cm samples to the diffusivity of the 100-Ω cm sample for 275–375 K. Column I is the diffusivity ratio of the majority carrier values while column II is the diffusivity ratio of the minority carrier values as determined in this work.

Temp. (K)	275		300		325		350		375	
ρ (Ω cm)	I	II	I	II	I	II	I	II	I	II
100	1.00	1.00	1.00	1.00	1.00	1.00	1.00	1.00	1.00	1.00
10	0.93	1.01(7)	0.95	0.99(7)	0.96	1.00(7)	0.97	1.02(7)	0.98	1.07(7)
2	0.83	0.89(6)	0.85	0.97(7)	0.88	0.97(7)	0.90	1.01(7)	0.92	1.05(7)
0.5	0.63	0.69(7)	0.67	0.76(8)	0.72	0.78(8)	0.76	0.80(8)	0.80	0.85(9)

The greatest uncertainty associated with the values of n_i calculated from band parameters arises from differences in interpreting the cyclotron resonance data used to calculate the valence-band density-of-states effective mass m_{dv}^*. Shown in Table II are three sets of values for the intrinsic carrier concentration[2] using the effective mass values of Madarasz *et al.*,[38] Humphreys,[39] and Hensel, from an unpublished work of Hensel cited by Humphreys.[39] It can be seen that there is quite good agreement with all values and excellent agreement with the values of Hensel ($<1\%$ difference). Due to the small uncertainties associated with the values presented here it would appear that the data of Hensel for m_{dv}^* are the most accurate.

However, the commonly cited value of 1.45×10^{10} cm^{-3} (Refs. 1, 3, and 4) for the intrinsic carrier concentration at 300 K is many standard deviations away from the figure reported here of $1.00(3)\times10^{10}$ cm^{-3}. Also, this result does not support the value of $\sim1.8\times10^{10}$ cm^{-3} deduced from earlier device measurements[5] using a high injection structure less suited to such measurements. The discrepancy between the present and the commonly cited value is 45% which introduces significant errors when modeling silicon devices. Currents in bipolar devices are proportional to n_i^2 and hence use of the larger value would lead to an overestimation of current by a factor of approximately 2. A recent review was unable to identify the origin of the larger value.[2] It would appear that there is no longer any justification for the continued use of this value.

From the present data it is also possible to independently derive accurate values of the ratio of the minority carrier mobility (or diffusivity) of one sample to that of another of different resistivity. Normalizing to the 100-Ω cm data, Eqs. (3) and (4) can be rearranged to give

$$\frac{\mu_n}{\mu_{n100}}=\frac{(I_{01}-I_{0e})}{(I_{01}-I_{0e})_{100}}\,\frac{N_A^-}{N_A^-\,100}\,\frac{W}{W_{100}}\,\frac{[\omega\coth\omega]_{100}}{[\omega\coth\omega]}. \quad (15)$$

The uncertainty associated with this ratio is estimated as being only 7% for the 10- and 2-Ω cm samples and 10% for the 0.5-Ω cm sample. Values are given in Table III for all temperatures along with 1σ uncertainties and are compared to the corresponding ratio of majority carrier mobilities as determined from Table I. At all temperatures the mobility ratio determined here is greater than the corresponding majority mobility ratio although the majority carrier value lies within, or close to the lower bound of the uncertainty associated with this extraction. At 300 K, assuming the 100-Ω cm sample has a mobility equal to the majority carrier value and the same uncertainty, estimations can be made of the mobilities of the other three samples. These results have been plotted in Fig. 5. For all samples the estimated minority carrier mobilities are greater than the majority values. A possible explanation for this increase has been put forward by Bennett.[40] As discussed previously, the decrease in μ_n as doping increases is due to the scattering of the electrons by the ionized dopant atoms. When electrons are the majority carriers this scattering is attractive while in the minority carrier case it is repulsive. Bennett suggests that the decrease in mobility will therefore be greatest for the majority carriers as the electrons will be scattered more effectively by the positively charged ionized dopant atoms. This would result in the minority mobility decreasing more slowly than the majority values as doping increases.

VI. CONCLUSIONS

Accurate measurement of the intrinsic carrier concentration of silicon has been made for temperatures in the range of 275 to 375 K from measurements of injected minority carrier flows in narrow base p-n junction diodes. The devices investigated were fabricated upon substrates with resistivities ranging from 0.5 to 100 Ω cm. The resulting determination of n_i was consistent for all resistivities. A value of 1.00×10^{10} cm^{-3} was determined at 300 K with an estimated one-standard-deviation uncertainty of only 3%. This value is in good agreement with the value of $1.08(8)\times10^{10}$ cm^{-3} deduced from measurements of band parameters and intrinsic conductivity measurements[2] and also with the value of 1.02×10^{10} cm^{-3} suggested by Wasserab.[7]

The commonly used value of 1.45×10^{10} cm^{-3} (Refs. 1, 3, and 4) at 300 K is not supported by the results presented here and appears to be in error. This difference is significant for silicon device analysis, particularly the modeling of solar cells. Use of the larger value would lead to an underestimation of the open-circuit voltage of a silicon photovoltaic device by ~20 mV. For bipolar devices, an overestimation of current flows at a given applied voltage by a factor of approximately 2 could be calculated using the larger value. The results for the temperature range 275–375 K are also in good agreement with the lower values reported in the literature.[2,7] The values of the intrinsic

carrier concentration of silicon determined in this work appear to be the most accurate reported to date. They also support the valence band effective mass parameters of Hensel, as reported by Humphreys.[39]

The results also suggest that minority carrier electrons in the present experimental configuration have higher mobilities than majority carriers in material with the same dopant concentration. This may be due to less effective scattering of conduction band electrons by ionized boron atoms than by ionized phosphorus atoms, as suggested by Bennett.[40]

ACKNOWLEDGMENTS

The authors acknowledge contributions of other members of the Centre for Photovoltaic Devices and Systems to this work and in particular Dr. J. Zhao who processed the devices. They also acknowledge the constructive input of Dr. Paul Basore and Dr. Ron Sinton to this work. This work was partly supported by the Australian Research Council and Sandia National Laboratories under Contract No. 75-0282. The Centre for Photovoltaic Devices and Systems is supported by the Commonwealth Special Research Centres Scheme. A.B.S. acknowledges the financial support of an Australian Postgraduate Research Award.

[1] S. M. Sze, *Physics of Semiconductor Devices,* 2nd ed. (Wiley, New York, 1981).
[2] M. A. Green, J. Appl. Phys. **67**, 2944 (1990).
[3] H. F. Wolf, *Semiconductors* (Wiley, New York, 1971).
[4] O. D. Trapp, R. A. Blanchard, and W. H. Shepperd, *Semiconductor Technology Handbook* (Technology Associates, Portola Valley, 1980); W. C. O'Mara, in *Semiconductor Materials and Process Technology Handbook,* edited by G. E. McGuire (Noyes, Park Ridge, 1988).
[5] A. Herlet and Z. Angew. Phys. **9**, 155 (1957).
[6] A. B. Sproul, M. A. Green, and J. Zhao, Appl. Phys. Lett. **57**, 255 (1990).
[7] Th. Wasserab, Z. Naturforsch. Teil A **32**, 746 (1977).
[8] M. A. Green, A. W. Blakers, J. Zhao, A. M. Milne, A. Wang, and X. Dai, IEEE Trans. Electron. Dev. **ED-37**, 331 (1990).
[9] I. Getreu, *Modeling the Bipolar Transistor* (Tektronix, Beaverton, OR, 1976).
[10] E. R. Cohen and B. N. Taylor, Codata Bull. **63**, 1 (1986).
[11] P. J. Chen, K. Misiakos, A. Neugroschel, and F. A. Lindholm, IEEE Trans. Electron. Dev. **ED-32**, 2292 (1985).
[12] J. C. Maxwell, *A Treatise on Electricity and Magnetism,* 3rd ed. (Clarendon, Oxford, 1892), Vol. 1.
[13] M. A. Green, A. W. Blakers, J. Zhao, A. Wang, A. M. Milne, X. Dai, and C. M. Chong, Report No. SAND 89-7041, Sandia National Laboratories, Albuquerque, Dec., 1989.
[14] R. B. Godfrey and M. A. Green, IEEE Trans. Electron. Dev. **ED-27**, 737 (1980).
[15] R. B. M. Girisch, R. P. Mertens, and R. F. De Keersmaeker, IEEE Trans. Electron. Dev. **ED-35**, 203 (1988).
[16] *Manual on the Use of Thermocouples in Temperature Measurement,* ASTM Special Technical Publication 470B (1981).
[17] W. R. Thurber, R. L. Mattis, and Y. M. Liu, *The Relationship Between Resistivity and Dopant Density for Phosphorus- and Boron-doped Silicon,* Nat. Bur. Stand., Spec. Publ. No. 400-64 (U.S. GPO, Washington, D.C., 1981).
[18] S. S. Li, Solid State Electron. **21**, 1109 (1978).
[19] J. A. del Alamo, in *Properties of Silicon,* EMIS Datareviews Series No. 4 (INSPEC, I.E.E., London, 1988).
[20] R. M. Swanson and S. E. Swirhun, Report No. SAND 87-7019, Sandia National Laboratories, Albuquerque, Nov., 1987.
[21] M. B. Prince, Phys. Rev. **93**, 1204 (1954).
[22] G. W. Ludwig annd R. L. Watters, Phys. Rev. **101**, 1699 (1956).
[23] M. Zerbst and W. Heywang, Z. Naturforsch Teil A **11**, 608 (1956).
[24] A. Neugroschel, IEEE Electron. Dev. Lett. **EDL-6**, 425 (1985).
[25] K. Misiakos and A. Neugroschel, IEEE Electron. Dev. Lett. **EDL-8**, 358 (1987).
[26] D. D. Tang, F. F. Fang, M. Scheuermann, T. C. Chen, and G. Sai-Halasz, *Proc. Int. Electron. Device Meeting, Los Angeles, CA, Dec., 1986* (IEEE, New York, NY, 1986), p. 20.
[27] J. Dziewior and D. Silber, Appl. Phys. Lett. **35**, 170 (1979).
[28] A. Skumanich, D. Fournier, A. C. Boccara, and N. M. Amer, Appl. Phys. Lett. **47**, 402 (1985).
[29] V. G. Weizer, C. K. Swartz, R. E. Hart, and M. P. Godlewski, IEEE Photovoltaic Specialists Conference, 1984, p. 117.
[30] D. C. Cronemeyer, Phys. Rev. **105**, 522 (1957).
[31] T. P. McLean and E. G. S. Paige, J. Phys. Chem. Solids **16**, 220 (1960).
[32] M. C. Carotta, M. Merli, L. Passari, and E. Susi, Appl. Phys. Lett. **49**, 44 (1986).
[33] W. M. Bullis, F. H. Brewer, C. D. Kolstad, and L. J. Swartzendruber, Solid State Electron. **11**, 639 (1968).
[34] ASTM Standards F84-88, *Annual Book of ASTM Standards,* Vol 10.05 (ASTM, Easton, MD, 1990).
[35] S. S. Li and W. R. Thurber, Solid State Electron. **20**, 609 (1977).
[36] A. Wang, J. Zhao, A. M. Milne, and M. A. Green (unpublished work).
[37] V. G. Weizer and R. De Lombard, Appl. Phys. Lett. **49**, 201 (1986).
[38] F. L. Madarasz, J. E. Lang, and P. M. Hemeger, J. Appl. Phys. **52**, 4646 (1981).
[39] R. G. Humphreys, J. Phys. C **14**, 2935 (1981).
[40] H. S. Bennett, Solid State Electron. **26**, 1157 (1983).